

Excitonic Coupling Modulated by Mechanical Stimuli

Alessandro Pirrotta,[†] Gemma C. Solomon,^{,†} Ignacio Franco,[‡] and Alessandro Troisi^{*,§}*

[†]Nano-Science Center and Department of Chemistry, University of Copenhagen, 2100
Copenhagen Ø, Denmark; [‡]Department of Chemistry, University of Rochester, Rochester, New
York 14627-0216, United States; [§]Department of Chemistry, University of Liverpool, L69 7DZ
Liverpool, United Kingdom

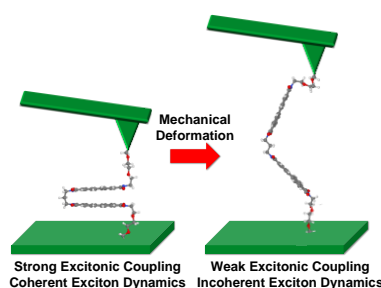
AUTHOR INFORMATION

Corresponding Author

gsolomon@nano.ku.dk, a.troisi@liverpool.ac.uk

ABSTRACT: Understanding energy transfer is of vital importance in a diverse range of applications from biological systems to photovoltaics. The ability to tune excitonic coupling in any of these systems, however, is generally limited. In this work, we have simulated a new class of single-molecule spectroscopy in which force microscopy is used to control the excitonic coupling between chromophores. Here we demonstrate that the excitonic coupling can be controlled by the mechanical manipulation of the molecule (perylene-3,4,9,10-tetracarboxylic diimide dimers and perylene-3,4,9,10-tetracarboxylic diimide-perylene-3,4,9,10-tetracarboxylic diimide heterodimers) and can be tuned over a broad range of values (0.02-0.15 eV) which correspond to different regimes of exciton dynamics going from the folded to the elongated structure of the dimer. In all the systems considered here, the switching from high to low coupling takes place simultaneously with the mechanical deformation detected by a strong increase and subsequent decay of the force. These simulations suggest that single-molecule force spectroscopy can be used to understand and eventually aid the design of excitonic devices.

TOC GRAPHICS



KEYWORDS

Exciton dynamics, single molecule force spectroscopy, excitonic switch, energy transfer, optoelectronic device.

Molecular excitonic systems are formed by aggregates of interacting chromophores.¹⁻³ Electronic excitations in these systems form excited states that can be localized or delocalized over several chromophores and evolve over time following coherent or incoherent energy transfer mechanisms, depending on the regime of transport. In organic materials, generally with low dielectric constants, the excited states are normally referred to as Frenkel excitons⁴ and can be understood as a linear combination of single electron excitations localized on individual chromophores. The dynamics of the excitons in molecular aggregates and, specifically, their coherent dynamics in ultra-fast processes is an important research focus in two distinct areas of physical sciences. The dynamics of the exciton formed in organic materials plays an important role in many optoelectronics devices including solar cells⁵⁻⁷ and light emitting diodes.⁸⁻¹⁰ Light harvesting complexes, used by plants and bacteria to transfer excitation energy to the photosynthetic center,¹¹⁻¹⁴ offer the opportunity to study the coherent time evolution of an excited state in a predetermined and known spatial arrangement of chromophores.¹⁵⁻¹⁷

The dynamics of the exciton in all cases is determined by the strength of the excitonic coupling, i.e. the interaction between the localized excitation (which is determined by the geometry), and the coupling of the exciton with the local nuclear modes, i.e. the exciton-environment coupling (which is partially controlled by the temperature). In all systems under investigation, there is very limited external control on the exciton dynamics and therefore little chance to design experiments to study exciton physics under different regimes or to exploit exciton dynamics to perform specific functions. Controlling the exciton coupling by external stimuli may lead to new optoelectronic devices, e.g. optomechanical switches. In the coherent exciton transport regime, the ability to control excitonic coupling can form the basis of new quantum information devices, where the

information is contained in the excitonic wave-function and the information processing takes place by controlling the excitonic Hamiltonian.^{18–21}

An opportunity to control the excitonic coupling is offered by the growing accuracy achievable in single-molecule force spectroscopy (SMFS),²² where mechanical stimuli can force a change in conformation in a molecular system (see Figure 1a). The most common force spectroscopies are magnetic tweezers,²³ optical tweezers²⁴ and atomic force microscopy (AFM.)^{25,26} AFM can be combined with other techniques to allow simultaneous measurement of, for example, current,²⁷ fluorescence spectroscopy^{28–30} infrared spectroscopy³¹ as well as optical tweezers combined with FRET,^{32,33} fluorescence microscopy³⁴ and other optical spectroscopy.³⁵ Specifically, in an AFM experiment, one end of a molecule is attached to a macroscopic surface and the other to an AFM tip (see Figure 1a) controlling the force exerted on the molecule.

The aim of this paper is to simulate a new variety of SMFS where both elongation force and excitonic coupling are simultaneously evaluated. The force spectroscopy allows the exploration of different conformations that the system can assume, while the excitonic coupling is evaluated, for example, from optical absorption or more complex time dependent techniques. This new SMFS opens the possibility to investigate excitonic physics at an unprecedented level of detail and to design *new excitonic devices* where the exciton dynamics is controlled externally.

A realistic model system. To test the potential of this SMFS, we consider systems consisting of two chromophores connected by a bridge where an external force is used to control the separation between the chromophores. Specifically, we investigate two classes of molecules: one formed by two perylenediimide units (PDI) and the other formed by one PDI and one terrylenediimide (TDI). The two chromophore units are connected through an aliphatic chain, the bridge, with n CH₂

groups (where n : {2-5}) and the extremities are each linked to an oxy-aliphatic chain, the linkers (see Figure 1b). These chromophores are suitable candidates for this experiment because of their optical stability, large extinction coefficients and high fluorescence quantum yields.³⁶ The overlap of the PDI emission and TDI absorption spectra makes this pair suitable for electronic energy transfer experiments.^{36,37}

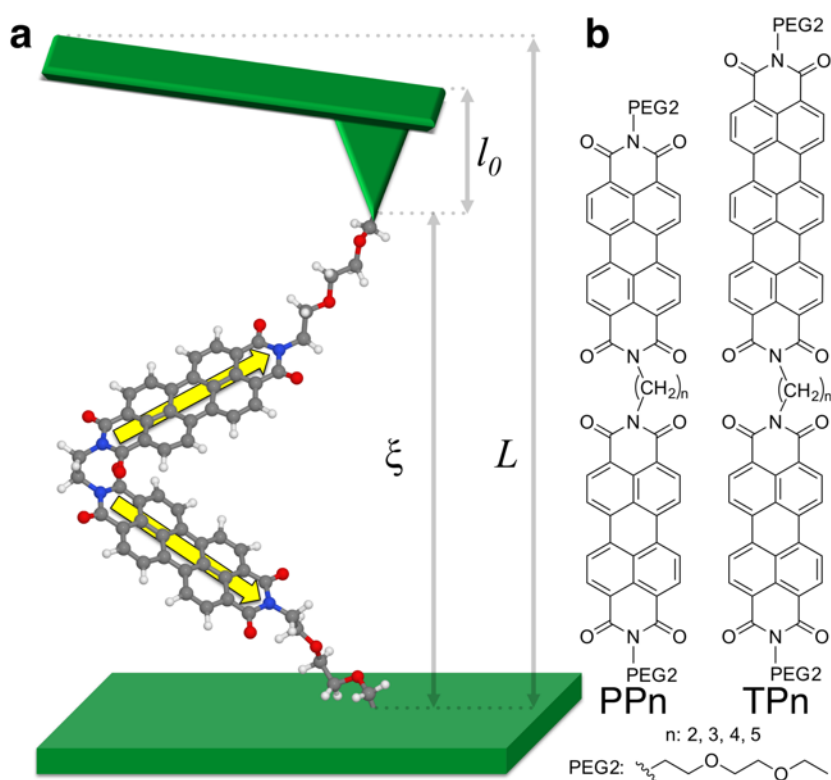


Figure 1. (a) Scheme of an AFM force spectroscopy setup. In these simulated experiments, the cantilever-surface distance (L) is controlled while the end-to-end molecular distance (ξ) thermally fluctuates. The spectroscopic properties of the molecule can be measured while simultaneously mechanically manipulating the intermolecular distance between the chromophores. The yellow arrows show the transition dipole moments. (b) Molecular structures of the systems investigated here. The **PP n** molecule is formed by two PDI molecules linked with a bridge of length n (e.g. panel a shows molecule **PP2**). **TP n** is formed by a TDI linked with a PDI. Both molecules are terminated with PEG linkers shown in the bottom panel.

The simulation of the pulling experiment is based on a constrained Molecular Dynamics (MD) scheme with details similar to those used in ref. 38–41 and provided in the Supporting Information

(SI). Briefly, the elongation is obtained by the application of a stiff isotropic potential on one terminal carbon atom which mimics the attachment to a surface, whilst the other terminal carbon is connected to a virtual harmonic spring, simulating the AFM cantilever. The excitonic coupling presented in the main manuscript is computed using the transition atomic charge method⁴² and therefore includes only the Coulombic contribution and will be indicated as J_C . To calculate the excitonic coupling, the PEG linkers and all the atoms of the bridge were removed from the conformations of the MD trajectory. The atomic transition charges were computed once using TD-DFT/LRC- ω PBEh/6-31G*⁴³ from an isolated PDI monomer, following the definition in eq. S1 of reference 42 (a full definition is also reported in the SI).⁴⁴ As shown in the SI we have verified that the contribution of short range interaction⁴⁵ is small and can be neglected for the system studied here and thus J_C provides a good estimate of the total exciton coupling.

Force and excitonic coupling spectroscopy. The results from the simulation of the force (F)-excitonic coupling spectroscopy for molecules **PP2** and **PP3** as a function of the end-to-end molecular length ξ are shown in Figure 2. The predominant conformations along the pulling experiment of both **PP2** and **PP3** are shown in Figure 3 (see also Figure S4, S5 and S6 in the Supporting Information for a more complete set of images). Consider first the force-excitonic spectroscopy of **PP2** (Figure 2a). At $\xi < 6$ Å the molecule is compressed which leads to a negative force. Upon elongation, the force depends weakly on the displacement (6 Å $< \xi < 15$ Å). In this region, the **PP2** conformations essentially form a quasi- π -stacked structure at $\xi = 5$ Å followed by a fully- π -stacked structure at $\xi = 12$ Å (Figure 3 top panel). Around $\xi = 20$ Å a force peak is observed: the increase in the force followed by its drop denotes a mechanical transition from a mechanically stable structure to another one. Before the transition, the molecule forms a stable

conformation ($\zeta = 17 \text{ \AA}$ Figure 3 top panel) as both potential energy U and the potential of mean force (PMF) ϕ (equivalent to the Helmholtz free energy) in Figure 2c show. At increased elongation, the applied force overcomes the π -stacking interactions and the molecule assumes a *gauche* conformation ($\zeta = 22 \text{ \AA}$ Figure 3 top panel). Overcoming the π -stacking interactions causes the increase in both free energy and potential energy.⁴⁶ This conformational change significantly affects the excitonic coupling (Figure 2e). Between $\zeta = 5\text{-}20 \text{ \AA}$, the average coupling oscillates around 0.14 eV. At the transition point, it drastically drops to $\sim 0.06 \text{ eV}$. Upon further elongation, another force peak signals a mechanical transition around $\zeta = 32 \text{ \AA}$: the weak π -stack interactions of the *gauche* conformation are stretched until the molecule is fully elongated (see conformations at $\zeta = 28 \text{ \AA}$ and 34 \AA). This region is also characterized by a concave region of the PMF, which indicates a mechanically unstable region. Here the intermediate coupling decreases until it reaches its minimum value as the PDI units are at the furthest possible distance.

Similarly a force peak indicates the π -stacked conformation breaking point for **PP3**. At this elongation, the excitonic coupling decreases, but contrarily to **PP2**, we find no intermediate region between the high and low coupling plateaus. This result is consistent with the finding of a single force peak at $\zeta = 22 \text{ \AA}$. Note the both larger breaking force and free energy difference of this system when compared to **PP2** (Figure 2 c and d). When the molecule is fully stretched, the low coupling plateau is now lower with respect to **PP2** due to the longer bridge which allows the PDI units to lie at a longer distance. Another difference is the increased stability of the π -stacked conformation of **PP3** with respect to **PP2**: the **PP2** π -stacked conformation is destabilized by both the strained N-C-C angles of the bridge and the repulsive interactions between the oxygen atoms. The excellent correlation between the critical points in the force spectroscopy and those in the excitonic coupling

map demonstrates that, by monitoring the force, one can control the magnitude of the excitonic coupling through mechanical deformation of the molecule.

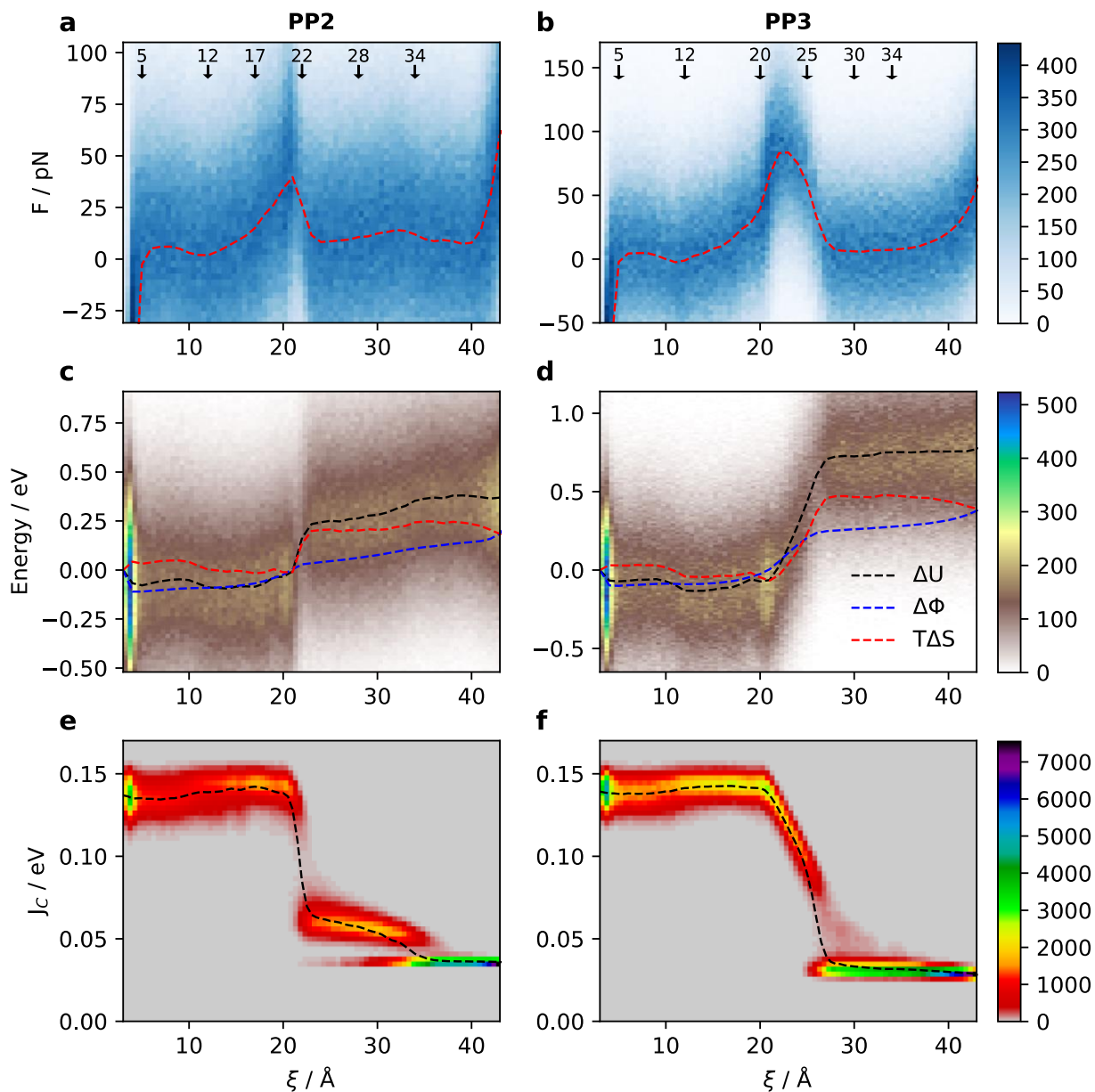


Figure 2. (a, b) 2D histograms of force vs. elongation. The dashed line indicates the force average. (c, d) 2D histogram of the relative potential energy and average value with dashed line. The entropy ΔS and Helmholtz free energy ϕ of the molecule is shown in red and blue dashed lines respectively. (e, f) 2D histograms of the absolute value of excitonic coupling. The dashed line shows the average values. The results for **PP2** and **PP3** are respectively shown on the left (a, c, e) and on the right (b, d, f). The color bar indicates the number of counts in bins of dimension $0.5 \text{ \AA} \times 3.5 \text{ pN}$ for (a-b),

$0.5 \text{ \AA} \times 0.01 \text{ eV}$ for (c-d), and $0.5 \text{ \AA} \times 0.003 \text{ eV}$ for (e-f). The averages are calculated with bins of dimension 1 \AA . The arrows in a and b refer to the structures in Figure 3.

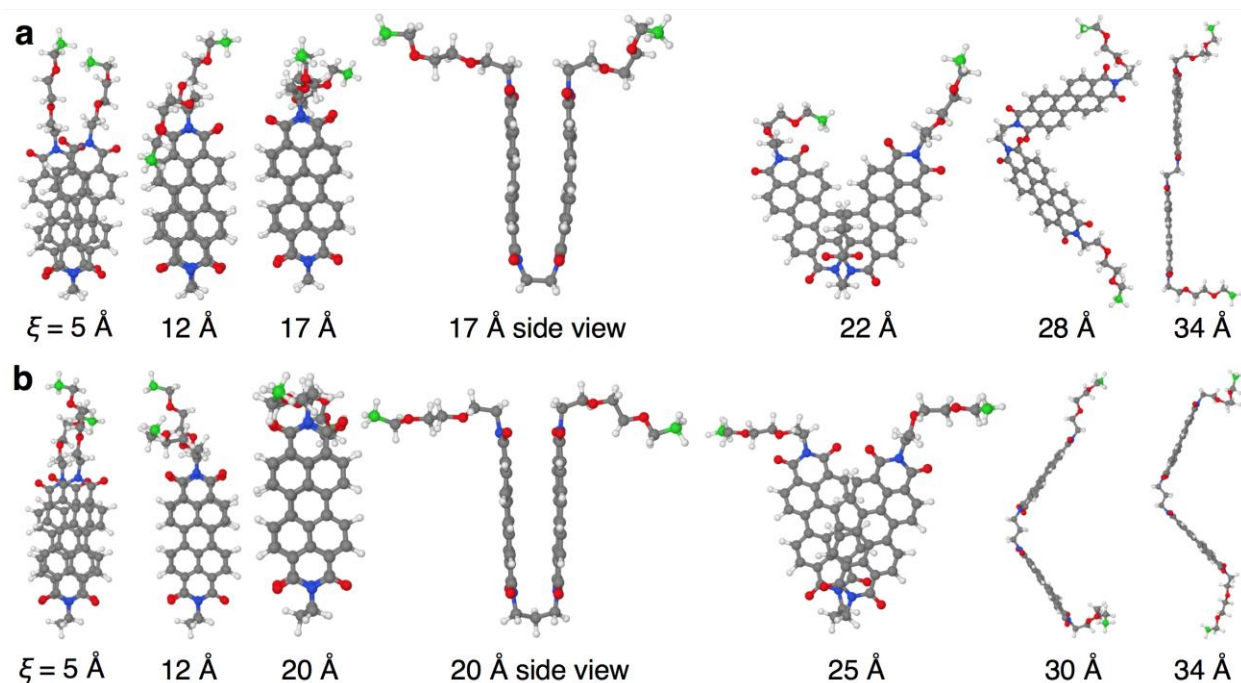


Figure 3. Representative structures along the pulling of **PP2** (top panel a) and **PP3** (bottom panel b) at different ξ . The constrained terminal carbon atoms are shown in green. The representative structures were obtained via a cluster analysis of conformations binned over 1 \AA .

Excitonic coupling change while pulling. Figure 4 shows the average force and the histogram of the excitonic coupling for molecule **PP2**, **PP3**, **PP4** and **PP5** versus the end-to-end molecular distance ξ . For all homo-dimers, the strong coupling regimes are measured in a region where the π -stacking interactions are strong and the free energy shows a mechanically stable phase (Supporting Information Figure S2). This demonstrates that the geometries responsible for a large coupling are not artifacts that come from non-physical structures. Note that the difference in free energy between 5 \AA and 12 \AA (the two stable conformers for short extensions) is smaller than the thermal energy for all molecules studied in this work (Supporting Information Figure S2 and S3). In all four cases, the major force peak is situated at the excitonic coupling switching region. The

position of the peak is constant as the bridge becomes longer: the breaking point is determined by the lengths of the PEG linkers (7.6 Å each and 3.6 Å for π -stack distance: a total of ca. 19 Å). The coupling switch is abrupt, i.e. from ~ 0.15 eV to ~ 0.03 eV over few Angstroms.

The range of excitonic coupling explored in the pulling experiment is not much affected by the bridge length (the lowest coupling slightly decreases for longer bridges), but the latter affects the conformational space of the chromophores units. Specifically, for **PP2** and **PP4** we find a region of intermediate coupling magnitude (labeled by I in Figure 4a and 4c), which is absent in either **PP3** or **PP5**. The force shows that a second breaking event takes place at longer ζ only for even n , while when n is odd we find only a single peak in the force. The reason for this is found by the different angle between the principal axis of the PDI units (see transition dipole moments sketched in Figure 1). When the π -stacked conformation is broken and n is 2 (even), the relative conformation of the CH₂ groups of the bridge changes from staggered to gauche. The dihedral angle increases as the molecule is stretched: this is the conformation responsible for the intermediate coupling. For $n = 3$ (odd) the CH₂ groups are already in gauche with respect to each other, thus stretching of the molecule causes the angle between the PDIs principal axes to increase (see transition dipole moments sketched in Figure 1) and the coupling decreases almost linearly until the CH₂ groups are forced to assume an all trans conformation which brings the PDI further apart (see Figure S4). The cluster analysis of the trajectories shows that after the first peak, an even number of CH₂ allows for long range π interactions while an odd number does not. This is due to the preferred all-trans conformation of an alkane chain, and the respective angle with the PDI units.

Generally, we find that the longer the bridge, the longer the average distance between the center of mass of the PDI units and thus the magnitude of the coupling in the the intermediate regime (labelled “I” in figure 4) decreases from $n = 2$ to $n = 4$. For $n = 4$ it is already difficult to distinguish

this region and the even-odd effect described above becomes less important. Note also the average force of the second peak for $n = 4$ is much lower than $n = 2$.

The length of the bridge affects also the coupling transition: the shorter the bridge, the sharper the drop of the coupling. As the bridge length increases, the transition between the high and the low coupling regime becomes smoother: this is attributed to a larger number of degrees of freedom available when the bridge is long.

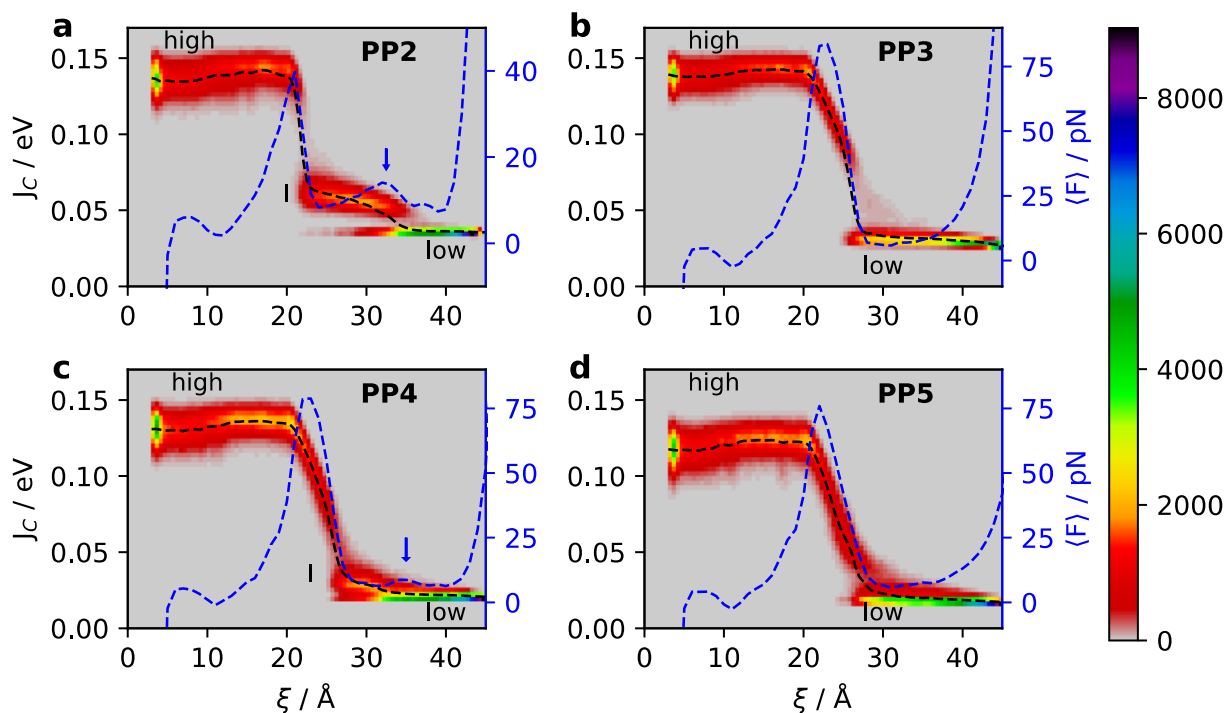


Figure 4. 2D histograms of the absolute value of excitonic coupling and force average for **PP n** with even n (left panel) and odd n (right panel), where $n = \{2, 3, 4, 5\}$. An intermediate coupling regime (I) is found only when the bridge is formed by an even number of CH_2 . An extra peak of the average force (blue arrow) is also found for even n , which signals another favorable conformation ensemble at longer ξ . The color bar indicates the number of counts in bins of dimension $0.5 \text{ \AA} \times 0.003 \text{ eV}$. The average force is calculated with bins of dimension 1 \AA .

The effect of the modulation of the excitonic coupling on the electronic and dynamical properties of the system depends on the regime of electron energy transfer.^{2,47} For strong coupling, exceeding the strength of exciton-vibration coupling, the system displays very delocalized excited states with no nuclear relaxation able to localize the excitation on one chromophore. Preparing an excited

state localized on a single chromophore in the high coupling limit would generate coherent dynamics (Rabi oscillations) between the chromophores. In the opposite, weak coupling, limit the excitons can become localized on a single chromophore by nuclear relaxation and the dynamics of exciton transfer would be incoherent, i.e. the excitation energy will hop between the two chromophores with a characteristic rate. The hopping barrier in the incoherent limit can be estimated as $\lambda/4$, where λ is the reorganization energy for the exciton transfer which, for the PDI molecule was evaluated computationally as 0.29 eV (See Supporting Information) in fair agreement with the value that can be extracted from the absorption/fluorescence spectra (e.g. 0.21 eV using the data from ref. ^{48,49} where the PDI is attached to a solubilizing group). When the excitonic coupling becomes comparable with the hopping barrier there is a transition between the incoherent and coherent regime and the exact quantum mechanical propagation becomes more complex. It is therefore remarkable that the range of excitonic coupling accessible through this experiment allows one to study the exciton dynamics close to the coherent regime (with minimal elongation and $J_C \sim 0.15$ eV) and in the purely incoherent regime (at large elongation and J_C in the ~ 0.01 – 0.03 eV range). Moreover, as the position of the force peak coincides with the strong to weak coupling switch, monitoring the force one can switch between coherent and incoherent regime via mechanical manipulation.

An additional difference between the high and low coupling configurations is the nature of the excited eigenstates (S_1 and S_2). To illustrate the spectroscopic differences at different elongations, we report simulated absorption spectra for the **PP2** and **PP5** systems in Figure 5 (see also Figure S8 in the SI). The spectra were obtained from the eigenstates $|a\rangle = \frac{1}{\sqrt{2}}(|1\rangle + |2\rangle)$, $|b\rangle = \frac{1}{\sqrt{2}}(|1\rangle - |2\rangle)$ of the excitonic Hamiltonian $H = E_{S_1}(|1\rangle\langle 1| + |2\rangle\langle 2|) + J_C(|1\rangle\langle 2| + |2\rangle\langle 1|)$, with $|1\rangle, |2\rangle$ the localized excitations states and $E_{S_1} = 2.79$ eV. The intensity of the transition from the ground

states to the excitonic eigenstates was computed as proportional to $|\langle 0|\mu|a\rangle|^2 = \frac{1}{2}|\mu_1 + \mu_2|^2$ and $|\langle 0|\mu|b\rangle|^2 = \frac{1}{2}|\mu_1 - \mu_2|^2$ with $\mu_1 = \langle 0|\mu|1\rangle$ and $\mu_2 = \langle 0|\mu|2\rangle$ (μ denotes the electric dipole operator and the matrix elements were computed for the isolated PDI molecules in the correct orientation and sign consistent with the evaluation of the coupling). In the high coupling – folded – configuration the chromophores will form an H-aggregate (with side-by-side transition dipole moments) while in the low coupling – elongated – configuration they form a J-aggregate (with head-to-tail transition dipole moments).⁵⁰ In the folded H-aggregate the S_1 absorption from the ground state would be almost forbidden and the S_2 would be intense and blue shifted with respect to the isolated chromophore. In the elongated J-aggregate, the S_1 absorption becomes intense and redshifted and S_2 absorption becomes forbidden. Fluorescence measurements can also indicate whether the chromophores are in the folded or elongated configuration: in the first case the fluorescence would be suppressed while in the second it would be enhanced. It should be noted that H- and J- character depends on the *relative* sign of J_C and the transition dipole moments (in our simulations the sign of J_C is constant and the H- and J- character is given by the relative orientation of μ_1 and μ_2).

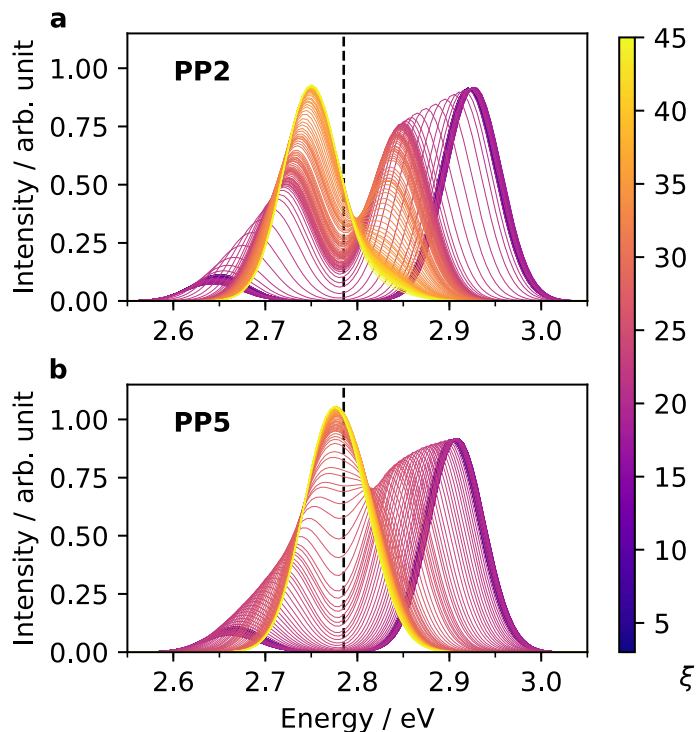


Figure 5. Simulated absorption spectra for **PP2** and **PP5** computed every 0.2 Å elongation using a Gaussian line shape with $\sigma = 0.03$ eV.

Force-spectroscopy can be applied also to heterodimers, for example TDI and PDI (see Figure 1b). In this case, there is an overlap between the emission spectrum of PDI and the absorption spectrum of the TDI which allows energy transfer from PDI to TDI following a selective excitation of the PDI molecule. The rate of energy transfer is controlled by the excitonic coupling,⁵¹ thus it is again possible to control the exciton dynamics through mechanical manipulation. An additional complication which will not be addressed in detail here is the presence of charge transfer (CT) states among the low energy lying states of the heterodimers. CT states were identified for molecule **TP2** for selected geometries at different elongations (Supporting Information Table S2). The CT energy levels are affected by the distance; thus, the energy of these excited states increases as the center of mass distance length between TDI and PDI increases. Also for the hetero-dimers (Figure 6) we find a high coupling regime at short elongation where the chromophores are in close

contact and strongly interacting. When the force signals a mechanical deformation, the coupling decreases and as the molecule is stretched further, the coupling drops to a low coupling plateau. We also find an extra mechanical deformation after the main force peak for both **TP2** and **TP4** and not for **TP3** and **TP5**. An intermediate coupling region is also seen for the even carbon atoms bridge **TPn** and it is not seen for the odd carbon atoms bridges, just like the **PPn** molecules. In contrast with **PPn** molecules, all the heterodimers show a larger coupling variance in the folded region. Specifically, the variance becomes larger as the bridge is longer. In fact, for a longer bridge there are more degrees of freedom which allows more conformations to be accessible, thus a larger spread in the coupling.

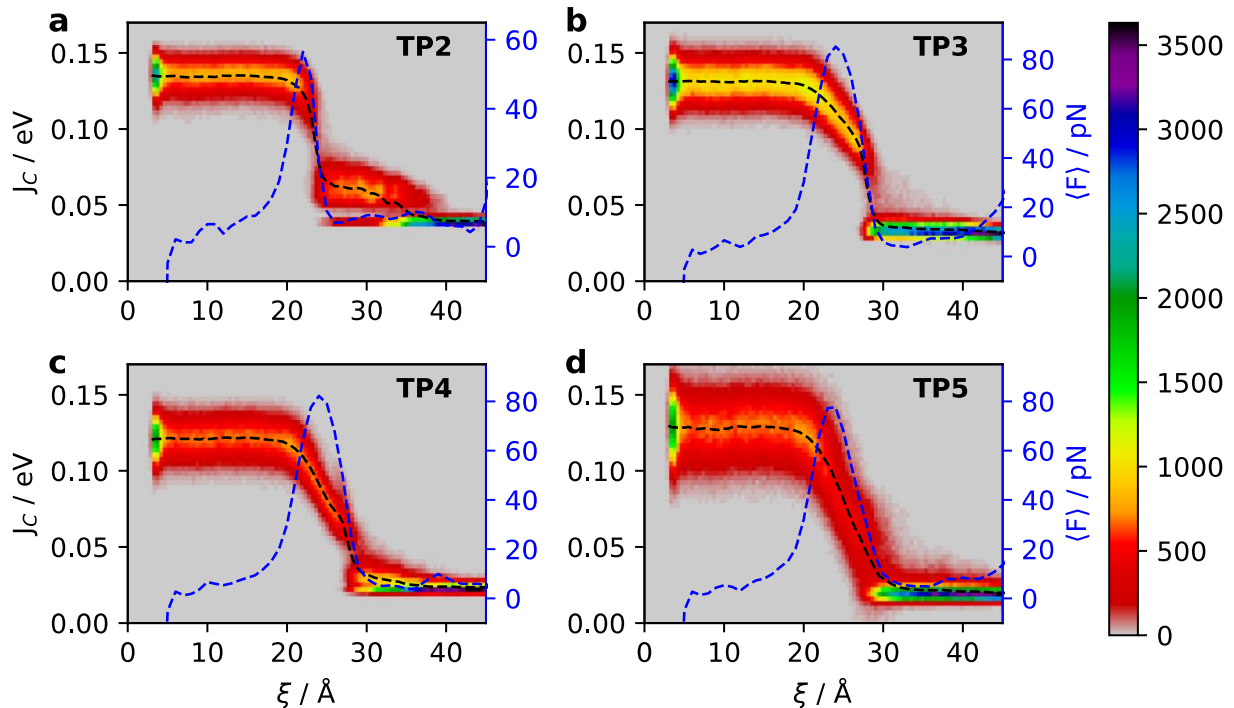


Figure 6. 2D histograms of excitonic coupling for the hetero system **TPn** with $n = \{2, 3, 4, 5\}$. The average force is more structured with respect to **PPn** molecules. The results are comparable and follow the same trend as **PPn** systems results. The color bar indicates the number of counts in bins of dimension $0.5 \text{ \AA} \times 0.003 \text{ eV}$. The average force is calculated with bins of dimension 1 \AA .

In conclusion, we have simulated a new class of single-molecule spectroscopy experiments in which force microscopy is used to control the excitonic coupling between chromophores in suitably designed dimers. Specifically, we have demonstrated that the exciton coupling can be varied over a broad range of values (0.02-0.15 eV) by the mechanical manipulation of the molecule. The stronger and weaker coupling correspond to different regimes of exciton dynamics and are found in correspondence with the folded and elongated structure of the dimer. These two conformations can also be detected optically (because they behave rather differently as H- and J-aggregates respectively) and, maybe more remarkably, from the force peak: in all the systems considered, the switch between high and low coupling regime corresponds to a strong increase of the force and subsequent drop. Relatively modest, but easy to rationalize, changes are observed when the length of the bridge between chromophores is changed, with a potentially interesting “intermediate” regime found for the $-(\text{CH}_2)_2-$ bridge. Most of the findings can be translated to the situation where two chromophores are different and their interaction is probed by the rate of energy transfer. Our findings suggest that a single-molecule force spectroscopy can be used to explore many subtleties of molecular exciton physics thanks to the potentially very accurate control achievable on the excitonic coupling.

ASSOCIATED CONTENT

Supporting Information. Computational methods for the simulation of the force spectroscopy and the computation of the excitonic coupling. Comparison of Coulombic excitonic coupling versus total excitonic coupling. Reorganization energy for PDI. PMF of all molecules investigated in this work. Representative conformations along the simulated pulling experiment for **PPn** molecules. Histogram of the angles between the transition dipole moments of the PDI

units for the **PPn** systems. Simulated absorption spectra for **PPn** systems. Charge transfer states for **TP2** at different elongations (PDF).

AUTHOR INFORMATION

Notes

The authors declare no competing financial interests.

ACKNOWLEDGMENT

A.P. and G.C.S. acknowledge financial support from the Danish Council for Independent Research, Natural Sciences, and the Carlsberg Foundation. IF acknowledge the support by the University of Rochester startup funds. AT acknowledges the support of ERC (Grant No. 615834).

REFERENCES

- (1) Scholes, G. D. Long-Range Resonance Energy Transfer in Molecular Systems. *Annu. Rev. Phys. Chem.* **2003**, *54* (18), 57–87.
- (2) Scholes, G. D.; Rumbles, G. Excitons in Nanoscale Systems. *Nat. Mater.* **2006**, *5* (9), 683–696.
- (3) Damjanović, A.; Kosztin, I.; Kleinekathöfer, U.; Schulten, K.; Damjanovi, A.; Kosztin, I.; Kleinekathö, U.; Schulten, K. Excitons in a Photosynthetic Light-Harvesting System: A Combined Molecular Dynamics, Quantum Chemistry, and Polaron Model Study. *Phys. Rev. E* **2002**, *65*, 31919.
- (4) Agranovich, V. *Excitations in Organic Solids*; Oxford University Press: Oxford, 2008.
- (5) Nozik, A. J.; Beard, M. C.; Luther, J. M.; Law, M.; Ellingson, R. J.; Johnson, J. C. Semiconductor Quantum Dots and Quantum Dot Arrays and Applications of Multiple Exciton Generation to Third-Generation Photovoltaic Solar Cells. *Chem. Rev.* **2010**, *110* (11), 6873–6890.
- (6) Günes, S.; Neugebauer, H.; Sariciftci, N. S. Conjugated Polymer-Based Organic Solar Cells. *Chem. Rev.* **2007**, *107* (4), 1324–1338.
- (7) Gregg, B. A. Excitonic Solar Cells. *J. Phys. Chem. B* **2003**, *107* (20), 4688–4698.
- (8) Taniyasu, Y.; Kasu, M.; Makimoto, T. An Aluminium Nitride Light-Emitting Diode with a Wavelength of 210 Nanometres. *Nature* **2006**, *441* (7091), 325–328.
- (9) Reineke, S.; Lindner, F.; Schwartz, G.; Seidler, N.; Walzer, K.; Lüssem, B.; Leo, K. White Organic Light-Emitting Diodes with Fluorescent Tube Efficiency. *Nature* **2009**, *459* (7244), 234–238.
- (10) Xu, T.; Zhang, Y. X.; Wang, B.; Huang, C. C.; Murtaza, I.; Meng, H.; Liao, L. S. Highly Simplified Reddish Orange Phosphorescent Organic Light-Emitting Diodes Incorporating a Novel Carrier- and Exciton-Confining Spiro-Exciplex-Forming Host for Reduced Efficiency Rolloff. *ACS Appl. Mater. Interfaces* **2017**, *9* (3), 2701–2710.
- (11) Cheng, Y.-C.; Fleming, G. R. Dynamics of Light Harvesting in Photosynthesis. *Annu. Rev. Phys. Chem.* **2009**, *60* (Copyright (C) 2012 American Chemical Society (ACS). All Rights Reserved.), 241–262.
- (12) Sarovar, M.; Ishizaki, A.; Fleming, G. R.; Whaley, K. B. Quantum Entanglement in Photosynthetic Light-Harvesting Complexes. *Nat. Phys.* **2010**, *6* (6), 462–467.
- (13) Scholes, G. D.; Fleming, G. R.; Olaya-Castro, A.; van Grondelle, R. Lessons from Nature about Solar Light Harvesting. *Nat. Chem.* **2011**, *3* (10), 763–774.
- (14) Curutchet, C.; Mennucci, B. Quantum Chemical Studies of Light Harvesting. *Chem. Rev.* **2017**, *117* (2), 294–343.

- (15) Herek, J. L.; Wohlleben, W.; Cogdell, R. J.; Zeidler, D.; Motzkus, M. Quantum Control of Energy Flow in Light Harvesting. *Nature* **2002**, *417* (6888), 533–535.
- (16) Lee, H.; Cheng, Y.-C.; Fleming, G. R. Coherence Dynamics in Photosynthesis: Protein Protection of Excitonic Coherence. *Science* (80-.). **2007**, *316* (5830), 1462–1465.
- (17) Collini, E.; Wong, C. Y.; Wilk, K. E.; Curmi, P. M. G.; Brumer, P.; Scholes, G. D. Coherently Wired Light-Harvesting in Photosynthetic Marine Algae at Ambient Temperature. *Nature* **2010**, *463* (7281), 644–647.
- (18) Reina, J. H.; Quiroga, L.; Johnson, N. F. Quantum Entanglement and Information Processing via Excitons in Optically Driven Quantum Dots. *Phys. Rev. A* **2000**, *62* (1), 1–8.
- (19) Troiani, F.; Hohenester, U.; Molinari, E. Exploiting Exciton-Exciton Interactions in Semiconductor Quantum Dots for Quantum-Information Processing. *Phys. Rev. B* **2000**, *62* (4), R2263(R).
- (20) Biolatti, E.; Iotti, R. C.; Zanardi, P.; Rossi, F. Quantum Information Processing with Semiconductor Macroatoms. *Phys Rev Lett* **2000**, *85* (26 Pt 1), 5647–5650.
- (21) Krenner, H. J.; Stuffer, S.; Sabathil, M.; Clark, E. C.; Ester, P.; Bichler, M.; Abstreiter, G.; Finley, J. J.; Zrenner, A. Recent Advances in Exciton-Based Quantum Information Processing in Quantum Dot Nanostructures. *New J. Phys.* **2005**, *7* (1), 184.
- (22) Neuman, K. C.; Nagy, A. Single-Molecule Force Spectroscopy: Optical Tweezers, Magnetic Tweezers and Atomic Force Microscopy. *Nat. Methods* **2008**, *5* (6), 491–505.
- (23) De Vlaminck, I.; Dekker, C. Recent Advances in Magnetic Tweezers. *Annu. Rev. Biophys.* **2012**, *41* (1), 453–472.
- (24) Moffitt, J. R.; Chemla, Y. R.; Smith, S. B.; Bustamante, C. Recent Advances in Optical Tweezers. *Annu Rev Biochem* **2008**, *77* (1), 205–228.
- (25) Binnig, G.; Quate, C. F.; Gerber, C. Atomic Force Microscope. *Phys. Rev. Lett.* **1986**, *56* (9), 930–933.
- (26) Giessibl, F. J. Advances in Atomic Force Microscopy. *Rev. Mod. Phys.* **2003**, *75* (3), 949–983.
- (27) Pobelov, I. V.; Mészáros, G.; Yoshida, K.; Mishchenko, A.; Gulcur, M.; Bryce, M. R.; Wandlowski, T. An Approach to Measure Electromechanical Properties of Atomic and Molecular Junctions. *J. Phys. Condens. Matter* **2012**, *24* (16), 164210.
- (28) Kassies, R.; Van Der Werf, K. O.; Lenferink, A.; Hunter, C. N.; Olsen, J. D.; Subramaniam, V.; Otto, C. Combined AFM and Confocal Fluorescence Microscope for Applications in Bio-Nanotechnology. In *Journal of Microscopy*; Blackwell Science Ltd, 2005; Vol. 217, pp 109–116.
- (29) Zhou, L.; Cai, M.; Tong, T.; Wang, H. Progress in the Correlative Atomic Force Microscopy

- and Optical Microscopy. *Sensors* **2017**, *17* (4), 938.
- (30) Fronczek, D. N.; Quammen, C.; Wang, H.; Kisker, C.; Superfine, R.; Taylor, R.; Erie, D. A.; Tessmer, I. High Accuracy FIONA-AFM Hybrid Imaging. *Ultramicroscopy* **2011**, *111* (5), 350–355.
 - (31) Dazzi, A.; Prater, C. B.; Hu, Q.; Chase, D. B.; Rabolt, J. F.; Marcott, C. AFM-IR: Combining Atomic Force Microscopy and Infrared Spectroscopy for Nanoscale Chemical Characterization. *Appl. Spectrosc.* **2012**, *66* (12), 1365–1384.
 - (32) Brenner, M. D.; Zhou, R.; Conway, D. E.; Lanzano, L.; Gratton, E.; Schwartz, M. A.; Ha, T. Spider Silk Peptide Is a Compact, Linear Nanospring Ideal for Intracellular Tension Sensing. *Nano Lett.* **2016**, *16* (3), 2096–2102.
 - (33) He, Y.; Lu, M.; Cao, J.; Lu, H. P. Manipulating Protein Conformations by Single-Molecule AFM-FRET Nanoscopy. *ACS Nano* **2012**, *6* (2), 1221–1229.
 - (34) Candelli, A.; Wuite, G. J. L.; Peterman, E. J. G. Combining Optical Trapping, Fluorescence Microscopy and Micro-Fluidics for Single Molecule Studies of DNA–protein Interactions. *Phys. Chem. Chem. Phys.* **2011**, *13* (13), 7263–7272.
 - (35) Hashemi Shabestari, M.; Meijering, A. E. C.; Roos, W. H.; Wuite, G. J. L.; Peterman, E. J. G. Recent Advances in Biological Single-Molecule Applications of Optical Tweezers and Fluorescence Microscopy. In *Single-Molecule Enzymology: Nanomechanical Manipulation and Hybrid Methods*; Elsevier Inc., 2017; Vol. 582, pp 85–119.
 - (36) Weil, T.; Vosch, T.; Hofkens, J.; Peneva, K.; Müllen, K. The Rylene Colorant Family-Tailored Nanoemitters for Photonics Research and Applications. *Angew. Chemie - Int. Ed.* **2010**, *49* (48), 9068–9093.
 - (37) Giaimo, J. M.; Lockard, J. V.; Sinks, L. E.; Scott, A. M.; Wilson, T. M.; Wasielewski, M. R. Excited Singlet States of Covalently Bound, Cofacial Dimers and Trimers of Perylene-3,4:9,10-Bis(dicarboximide)s. *J. Phys. Chem. A* **2008**, *112* (11), 2322–2330.
 - (38) Franco, I.; Ratner, M. A.; Schatz, G. C. Single-Molecule Pulling: Phenomenology and Interpretation. In *Nano and Cell Mechanics*; John Wiley & Sons, Ltd: Chichester, UK, 2012; Vol. 3113, pp 359–388.
 - (39) Franco, I.; Schatz, G. C.; Ratner, M. A. Single-Molecule Pulling and the Folding of Donor-Acceptor Oligorotaxanes: Phenomenology and Interpretation. *J. Chem. Phys.* **2009**, *131* (12), 124902.
 - (40) Pirrotta, A.; Solomon, G. C.; Franco, I. Hydrogen Bonding in Tight Environments: Simulated Force Spectroscopy of Nanoconfined Hydrogen-Bonded Complexes. *J. Phys. Chem. C* **2016**, *120* (34), 19470–19478.
 - (41) Pirrotta, A.; De Vico, L.; Solomon, G. C.; Franco, I. Single-Molecule Force-Conductance Spectroscopy of Hydrogen-Bonded Complexes. *J. Chem. Phys.* **2017**, *146* (9), 92329.
 - (42) Aragón, J.; Troisi, A. Excitonic Couplings between Molecular Crystal Pairs by a Multistate

- Approximation. *J. Chem. Phys.* **2015**, *142* (16), 164107.
- (43) Rohrdanz, M. A.; Martins, K. M.; Herbert, J. M. A Long-Range-Corrected Density Functional That Performs Well for Both Ground-State Properties and Time-Dependent Density Functional Theory Excitation Energies, Including Charge-Transfer Excited States. *J. Chem. Phys.* **2009**, *130* (5), 54112.
- (44) We have verified that the variation of the transition dipole moment by performing the calculation with different density functionals is modest with respect to the effect observed. For example, the transition dipole momenta obtained from CAM-B3LYP, LC-PBE0 and LC-BLYP are respectively 0.5 %, 2 % and 1% larger than the one obtained with LRC- ω PBEh (the same basis set 6-31G* was used).
- (45) Fornari, R. P.; Rowe, P.; Padula, D.; Troisi, A. Importance and Nature of Short-Range Excitonic Interactions in Light Harvesting Complexes and Organic Semiconductors. *J. Chem. Theory Comput.* **2017**, *13* (8), 3754–3763.
- (46) Typically, the energy and entropy show more structure than the PMF as the two components partially cancel one another, leading to only modest changes in the PMF. The reason why minima in internal energy U do not necessarily show up as minima in the PMF is because when stabilizing interactions are maximized (leading to a reduced value of U) the range of molecular motion typically decreases, leading to a reduced entropy that partially cancels the stabilization due to interactions.
- (47) Aragón, J.; Troisi, A. Regimes of Exciton Transport in Molecular Crystals in the Presence of Dynamic Disorder. *Adv. Funct. Mater.* **2016**, *26* (14), 2316–2325.
- (48) Seibt, J.; Marquetand, P.; Engel, V.; Chen, Z.; Dehm, V.; Würthner, F. On the Geometry Dependence of Molecular Dimer Spectra with an Application to Aggregates of Perylene Bisimide. *Chem. Phys.* **2006**, *328* (1–3), 354–362.
- (49) Kistler, K. A.; Pochas, C. M.; Yamagata, H.; Matsika, S.; Spano, F. C. Absorption, Circular Dichroism, and Photoluminescence in Perylene Diimide Bichromophores: Polarization-Dependent H- and J-Aggregate Behavior. *J. Phys. Chem. B* **2012**, *116* (1), 77–86.
- (50) Spano, F. C. The Spectral Signatures of Frenkel Polarons in H- And J-Aggregates. *Acc. Chem. Res.* **2010**, *43* (3), 429–439.
- (51) Truong, K.; Ikura, M. The Use of FRET Imaging Microscopy to Detect Protein-Protein Interactions and Protein Conformational Changes in Vivo. *Curr. Opin. Struct. Biol.* **2001**, *11* (5), 573–578.